sustainability

MDPI

Article

Hydraulic Performance of an Innovative Breakwater for Overtopping Wave Energy Conversion

Claudio Iuppa [1,*], Pasquale Contestabile [2], Luca Cavallaro [1], Enrico Foti [1] and Diego Vicinanza [2,3]

[1] Department of Civil Engineering and Architecture, University of Catania, Via Santa Sofia 64, 95123 Catania, Italy; luca.cavallaro@dica.unict.it (L.C.); efoti@dica.unict.it (E.F.)

[2] Dipartimento di Ingegneria Civile, Design, Edilizia e Ambiente, Seconda Università degli Studi di Napoli. Via Roma 29, 81031 Aversa (Caserta), Italy; pasquale.contestabile@unina2.it (P.C.); diego.vicinanza@unina2.it (D.V.)

[3] CONISMA—National Inter-University Consortium of Marine Sciences, Piazzale Flaminio 9, 00196 Roma, Italy

* Correspondence: ciuppa@dica.unict.it

Academic Editors: Mariano Buccino and Gregorio Iglesias Rodriguez
Received: 30 September 2016; Accepted: 20 November 2016; Published: 25 November 2016

Abstract: The Overtopping BReakwaterfor Energy Conversion (OBREC) is an overtopping wave energy converter, totally embedded in traditional rubble mound breakwaters. The device consists of a reinforced concrete front reservoir designed with the aim of capturing the wave overtopping in order to produce electricity. The energy is extracted through low head turbines, using the difference between the water levels in the reservoir and the sea water level. This paper analyzes the OBREC hydraulic performances based on physical 2D model tests carried out at Aalborg University (DK). The analysis of the results has led to an improvement in the overall knowledge of the device behavior, completing the main observations from the complementary tests campaign carried out in 2012 in the same wave flume. New prediction formula are presented for wave reflection, the overtopping rate inside the front reservoir and at the rear side of the structure. Such methods have been used to design the first OBREC prototype breakwater in operation since January 2016 at Naples Harbor (Italy).

Keywords: wave energy converters; rubble mound breakwater; wave overtopping; wave reflection

1. Introduction

Energy consumption has been one of the most salient ways of measuring progress in society. This is especially true nowadays: fossil fuel is not only a cultural phenomenon; it is an economic necessity for many developing/developed countries. However, new parameters, such as energy efficiency, are beginning to be used to estimate the well-being of individual states. In this contest, the renewable energy share of global consumption represents a world-wide index by which it is possible to assess the technological advancement of a country.

Among the various renewable energy sources, ocean energy has attracted the attention of the business and scientific community from as early as 1973. The main reason is that the resource is so vast [1,2], i.e., the theoretical potential resource of ocean energy is more than sufficient to meet present and projected global electricity demands well into the future.

In the last decade, numerous research projects aimed both at evaluating the potential energy and also designing new types of converters (called Wave Energy Converters (WECs)) were carried out. This interest is motivated by the various advantages that characterize such a source [3]: the high energy density, greater than that of solar and wind; the easy prediction of the wave characteristics through numerical models [4,5]; the reduced energy loss during wave propagation in relative water depth. However, these benefits are offset by the following drawbacks: the high variability of the wave

characteristic through time [6]; WECs are exposed to large environmental forces; high production costs compared to other devices as photovoltaic and wind turbines [7].

A solution to significantly decrease the costs would be to develop hybrid devices that can be embedded within coastal or offshore infrastructures [8–10]. This important new concept for coastal defense structures could be a realistic solution for the WEC systems to become economically competitive with other renewable energy devices, especially considering the fact that they can be integrated within existing breakwaters or by upgrades. This integration has several advantages from an economical, constructional and operational point of view. Construction costs are shared, and the access to construction, operation and maintenance of the devices would become much easier. Among the large number of WEC technologies, only very few devices have been constructed at the prototype scale, and not one is at the commercial stage.

The utilization of wave energy close to the shoreline is attractive thanks to reduced costs concerning construction, access, maintenance and grid connection. On the other hand, the available wave energy is less than at deep water sites, although recent work (e.g., [11–13]) demonstrated that there are sites where energy is concentrated due to wave transformation phenomena, such as wave refraction.

Following the concept of the integration of WECs in a breakwater and starting from previous works on WEC systems, such as Wave Dragon [14] and the Sea-wave Slot-cone Generator [15–21], an innovative built integrated device called OBREC (Overtopping BReakwater for Energy Conversion [8]) has been operating since January 2016 (Figure 1a,b) [22].

OBREC is a nearshore device combining rubble mound breakwaters with WECs. The device is able to extract energy through the wave overtopping phenomenon. Instead of dissipating the incoming wave energy on the breakwater armor layer, OBREC uses a concrete ramp in order to increase the overtopping discharge and a front reservoir designed to capture the wave overtopping in order to convert wave energy into potential energy. Water stored in the reservoir produces energy by flowing through low head hydraulic turbines, using the difference in water level between the reservoir and the main sea water level (Figure 1c).

To estimate the hydraulic and the structural performance of OBREC, 2D physical model tests were carried out at Aalborg University (DK) in 2012 (AAU12) [8,11,23].

The AAU12 tests were aimed at estimating the main differences between a traditional rubble mound breakwater and OBREC. Two different configurations, characterized by different ramp lengths, respectively, 7.5 cm and 12.5 cm at the model scale, were tested. Hydraulic results showed that the integration of the device in a traditional breakwater improves the overall performances [8]. As regards the hydraulic performances, the main results are:

(1) the device shows a similar or even reduced reflection coefficient with respect to traditional rubble mound breakwater;
(2) overtopping at the rear side of the structure is reduced by adopting appropriate precautions, e.g., the realization of a parapet at the crest of the OBREC crown wall;
(3) new design methods have been proposed for the estimation of the reflection coefficient, overtopping at the rear side of the structure and overtopping volume in the front reservoir.

However, the influence of some factors were not evaluated during the AAU12 tests. Indeed, the AAU12 tests did not allow for an understanding of how the hydraulic performance (reflection and wave overtopping) could be affected by the following geometrical characteristics: reservoir width, frontal ramp length and frontal ramp shape. In order to evaluate the influence of such parameters in the hydraulic performances of the device, new tests (AAU14) were carried out.

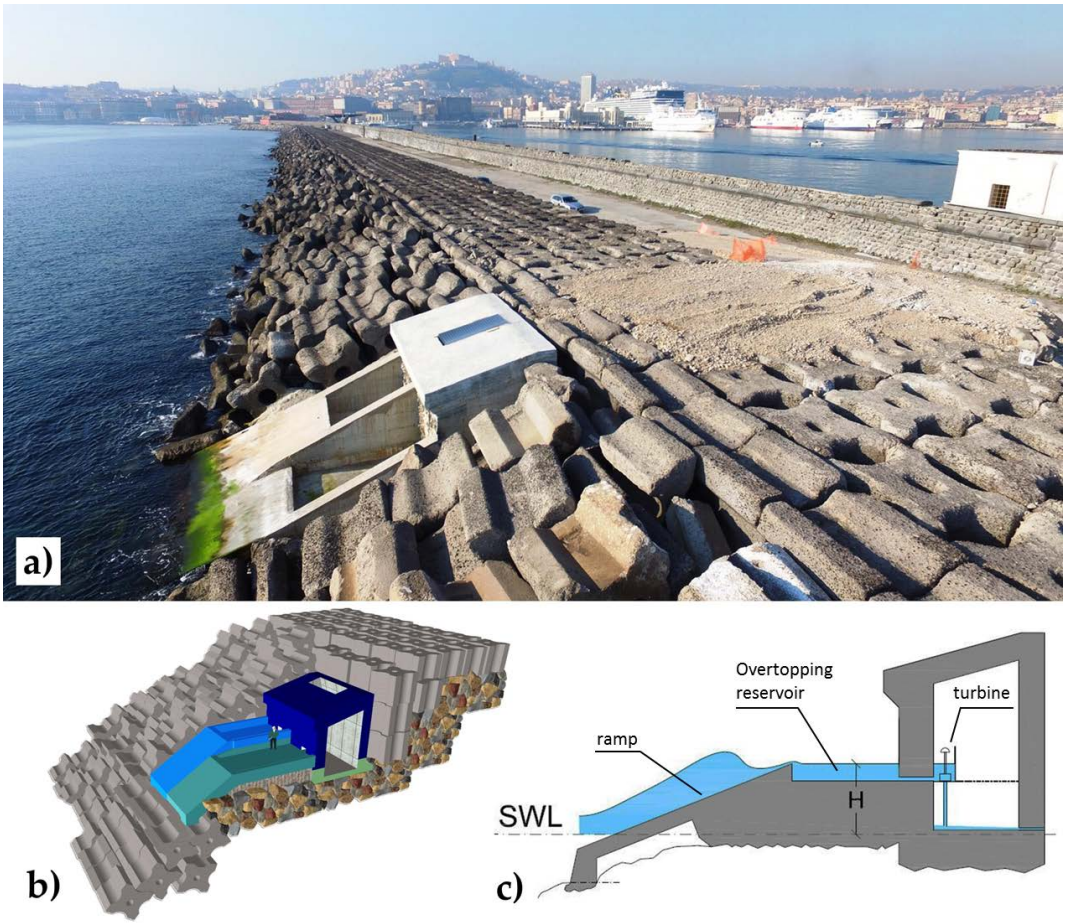

Figure 1. OBREC prototype at Naples Harbor: (**a**) prototype photo; (**b**) prototype structural components; (**c**) working principle (where SWL indicates the still water level).

The AAU14 tests were carried out at the Hydraulic and Coastal Engineering Laboratory of Aalborg University at a length scale of 1:30 (Froude scaling) compared to typical prototype dimensions. Different geometric configurations were investigated by varying the width of the reservoir, the water level and the profile of the frontal ramp. A few preliminary results on hydraulic performances have already been presented by Iuppa et al. [24].

This paper is organized as follows: Section 2 provides information on the experimental procedure and setup. In Section 3, the hydraulic performances of the device are evaluated: the reflection coefficient of the structure, overtopping at the rear side of the structure and the overtopping volume in the front reservoir. Section 4 is devoted to an overall discussion with some concluding remarks.

2. Experimental Procedure and Setup

2.1. Wave Flume

The model tests were carried out at the Hydraulic and Coastal Engineering Laboratory of Aalborg University at a length scale of 1:30 (Froude scaling) compared to the typical prototype dimensions. The wave flume is 25 m long, 1.50 m wide and 1.20 m deep. The flume configuration is shown in Figure 2.

Moving from the paddle (a hydraulic-driven piston mode generator) to the model, the bottom was horizontal for the first 6.5 m, with a 3.5-cm step, a 1:98 slope section with a length of 9 m and, finally, a horizontal section where the model was placed. The flume was divided into two sub-flumes by a guiding wall in order to test two different device configurations. Each part was 0.73 m wide.

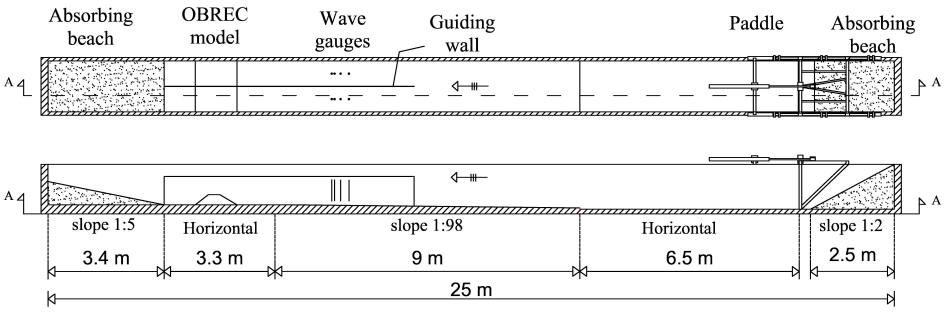

Figure 2. Plant and cross-section of the wave flume. OBREC, Overtopping BReakwater for Energy Conversion.

2.2. Tested Configurations

The tests were performed by varying: (i) the shape of the frontal ramp; (ii) the height of the frontal ramp, R_r, with respect to the still water level (SWL); (iii) the width of the frontal reservoir.

Figure 3 shows the cross-section of the analyzed configurations in the AAU14 tests. In the figure: B_r is the reservoir width; B_s is the emerged sloping plate width; ΔB_{rs} is the horizontal distance between the crown wall and the crest of the ramp; h_r is the depth reservoir; R_c is the crest free-board of the crown wall; R_r is the crest free-board of the front reservoir; ΔRc is the vertical distance between the crown wall and the crest of the ramp; d_w is the height of the sloping plate; d_d is the height of the submerged sloping plate; h is the water depth at the toe of the structure.

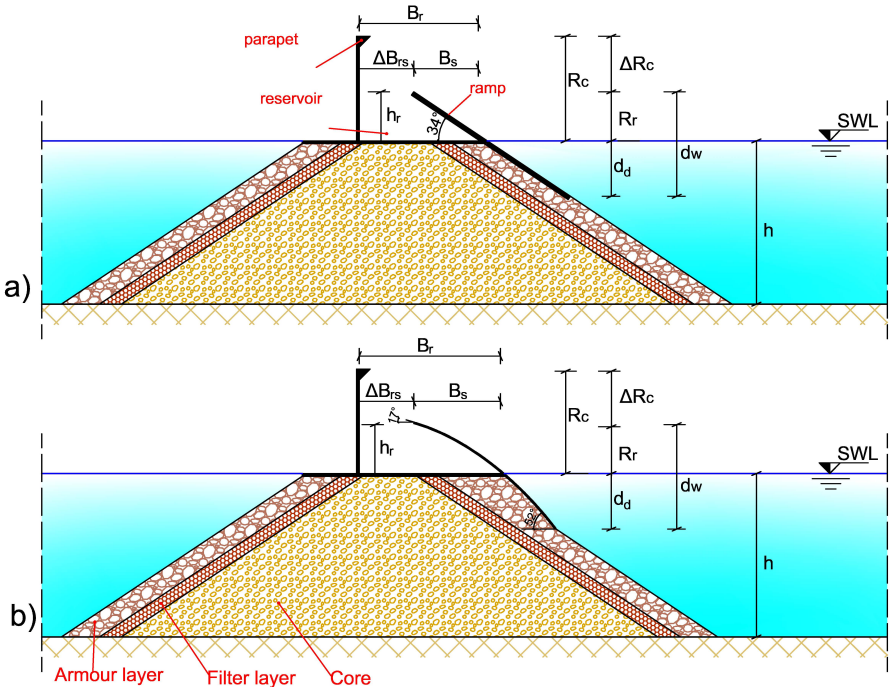

Figure 3. Cross-section of the analyzed configuration: (**a**) flat configuration (α equal to 34°); (**b**) curved configuration (α varies linearly between 52° and 17°).

As regards the shape of the frontal ramp, two different configurations were tested: the first (defined as the flat configuration) was characterized by a flat ramp with a slope angle of 34°; the second (the curved configuration) has a curvilinear ramp where the slope angle varies linearly between 52° and 17°. The slope of the flat ramp was driven by Kofoed [25] where a maximization of the amount of overtopping was observed for such a geometry. The curved configuration was tested in order to verify

for the on shore condition the results of Kofoed [26]. In this study, performed for the offshore wave condition, such a geometry maximize the overtopping discharge.

The height of the frontal ramp R_r with respect to the s.w.l. influences the energy conversion. Indeed, a low values of R_r produces high overtopping discharge in the front reservoir, but at the same time results in low hydraulic head on the turbine. The other way around, high values of R_r produce small discharge in the reservoir and high hydraulic head. Typical values of R_r are in the range of 1–3.5 m. Furthermore, the study of the response of the system to R_r variation is relevant in order to evaluate the influence of tide.

The width of the front reservoir ΔB_{rs} can influence the overtopping discharge trough the overall structure. Typical values of ΔB_{rs} are in the range of 5–15 m.

The model geometrical characteristic are shown in Table 1 together with those of the AAU12 tests. A total of 9 cases were analyzed for each configuration.

Table 1. Geometrical characteristics of the different configuration tested. The values refer to the Aalborg University 2014 (AAU14) and AAU12 tests.

	AAU14		AAU12
	Flat Configuration	**Curved Configuration**	**Flat Configuration**
h_r (m)	0.090	0.094	0.100
B_s (m)	0.119	0.160	0.534
ΔB_{rs} (m)	0.100, 0.200, 0.300	0.100, 0.200, 0.300	0.415, 0.488
d_w (m)	0.192	0.192	0.075, 0.125
R_r (m)	0.045 ($R1$), 0.095 ($R2$), 0.125 ($R3$)	0.049 ($R1$), 0.099 ($R2$), 0.129 ($R3$)	0.035–0.155
Δ_{Rc} (m)	0.102	0.098	0.045–0.165

Hereafter, the symbols $R1$, $R2$ and $R3$ are used to indicate the three different values of R_r.

In order to reduce the overtopping discharge through the overall structure, a parapet has been placed on the top of the upper crown wall (Figure 4). Indeed, as indicated by Vicinanza et al. [8] the presence of a "nose" causes a strong reduction of the overtopping at the rear side of the model. The parapet had the shape of an isosceles triangle with vertical and horizontal sides of 2 cm in the model scale. Such dimensions were defined on the basis of the authors' experience.

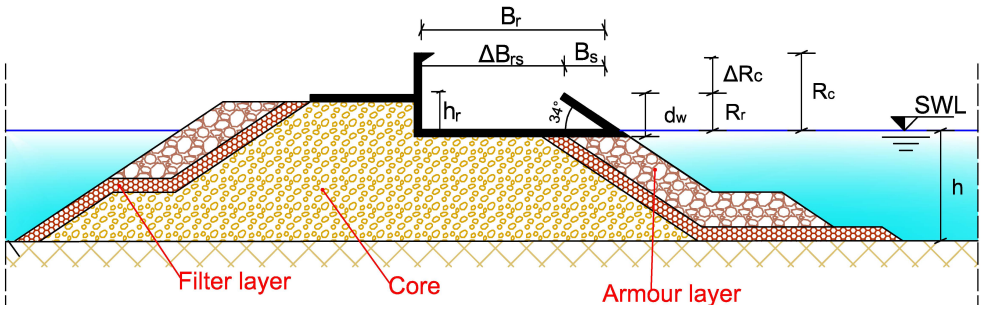

Figure 4. OBREC configuration in the AAU12 tests after Vicinanza et al. [8].

The rubble mound material was chosen in order to ensure the stone stability under wave action and to reproduce the main hydraulic behavior of the structure. The equivalent cube side length exceeding by 50% the stones ($D_{n,50}$) for the armor layer was 50 mm. In order to reproduce the turbulent flow inside the filter layer, a $D_{n,50}$ equal to 20 mm was assumed in such a layer. Finally, the $D_{n,50}$ was equal to 5 mm for the core, in order to prevent the washing of the core material.

2.3. Wave Characteristics

Waves were generated from a hydraulically-driven piston mode generator controlled by the software AwaSys developed by Aalborg University. Simultaneously, active absorption of reflected

waves was used in all tests [27]. Waves were generated based on the three parameters in the JONSWAP (JOint North Sea Wave Project) spectrum: significant wave height H_{m0}, peak period (T_p) and the peak enhancement factor γ (γ = 3.3 in all tests). Each test contained at least 1000 waves.

The data obtained from the eight wave gauges (four for the model) were analyzed with the software WaveLab (developed at Aalborg University). The software allowed one to estimate the wave characteristics (e.g., incident wave height, reflected wave height, energy wave period) with the method of Zelt and Skjelbreia [28]. A total of 200 tests was carried out.

Table 2 shows the maximum and minimum values of the water level and of the wave characteristics estimated at the models' toe.

Table 2. Maximum and minimum values of the water level and wave characteristics at the models' toe evaluated trough the method of Zelt and Skjelbreia [28].

	h (m)		H_{m0} (m)		$T_{m-1,0}$ (s)		$L_{m-1,0}$ (m)	
	min	max	min	max	min	max	min	max
ΔB_{rs} = 0.1 m	0.27	0.35	0.02	0.12	0.76	2.2	0.92	7.56
ΔB_{rs} = 0.2 m	0.27	0.35	0.05	0.13	0.76	2.2	0.92	7.56
ΔB_{rs} = 0.3 m	0.27	0.35	0.05	0.118	0.77	2.2	0.93	7.57

Table 3 reports the range of some dimensionless parameters. $L_{m-1,0}$ and $\xi_{m-1,0}$ represent the wavelength and the breaker parameter, respectively, referenced to the spectral incident energy wave period $T_{m-1,0}$.

Table 3. Dimensionless tested parameter ranges.

		ΔB_{rs} = 0.1 m	ΔB_{rs} = 0.2 m	ΔB_{rs} = 0.3 m
$H_{m0}/L_{m-1,0}$	min	0.016	0.015	0.015
	max	0.031	0.033	0.031
H_{m0}/h	min	0.07	0.061	0.069
	max	0.500	0.479	0.479
R_r/H_{m0}	min	0.370	0.370	0.399
	max	2.344	2.528	2.280
R_c/H_{m0}	min	1.120	1.110	1.970
	max	6.020	6.890	6.130
$B_r/L_{m-1,0}$	min	0.035	0.049	0.064
	max	0.284	0.388	0.497
$h/L_{m-1,0}$	min	0.037	0.039	0.037
	max	0.382	0.377	0.378
$\xi_{m-1,0}$	min	3.910	3.890	3.940
	max	5.750	5.720	5.770

2.4. Instruments

The laboratory campaign was carried out in order to gather data on the following characteristics: wave reflection, wave loading, wave overtopping discharge both in the front reservoir and behind the whole structure.

In each sub-flume, the following instruments were installed: 4 resistance wave gauges in order to evaluate incident and reflected wave spectra; 2 boxes to collect the water discharge in the front reservoir and behind the whole structure; 2 depth gauges, protected by hollow cylinders in PVC in order to measure the overtopping discharge; 14 pressure transducers for the estimation of the pressures/forces induced by the waves on the structure.

The distance between the models and the wave gauges was approximately 2.80 m (Figure 2), according to the recommendations of Klopman and van der Meer [29].

In each overtopping accumulation box, a water level gauge was installed in order to measure overtopping discharge and to control evacuation pumps (Figure 5). The overtopping accumulation box was connected to the frontal reservoir by a PVC pipe, while the rear side-overtopping accumulation box received the discharge through a ramp placed on the top of the crown wall. The PVC pipe outflow was set at the same level of the reservoir bottom.

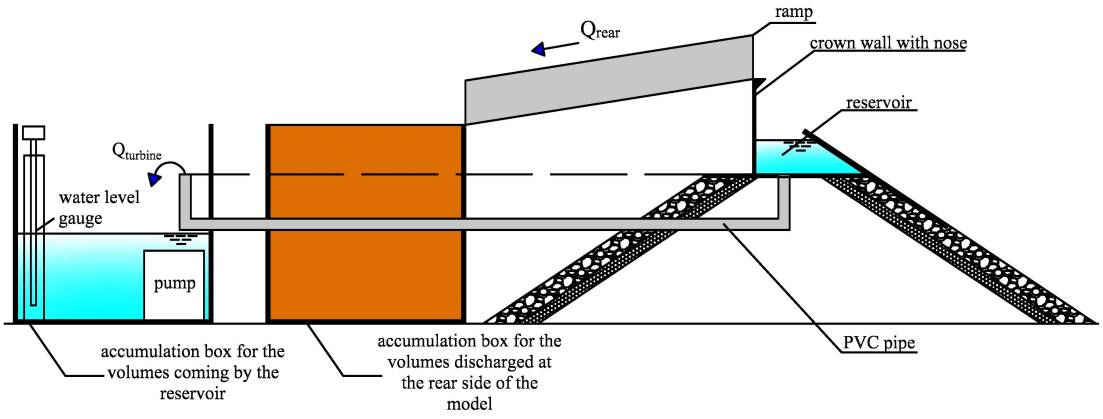

Figure 5. Wave-by-wave system for flow discharge measurement.

Overtopping discharges at the rear side of the models and in the front reservoirs were estimated using the water level gauge measurements. Once the water level inside the box is known, it is possible to estimate the flow rate Q as:

$$Q = \frac{\Delta V}{\Delta t} = \frac{A(h) \times (h_{box}(t + \Delta t) - h_{box}(t))}{\Delta t} \quad (1)$$

where ΔV is the overtopping volume variation in the Δt, $A(h)$ is the cross-sectional area of the box and h_{box} is the water level. The area $A(h)$ is a function of the water level due to the presence of the pipes and pump used to extract the water. $A(h)$ was estimated by measuring the water depth in the box after a known water volume was introduced in the box.

3. Results

The overtopping discharge Q_{in} through Section S_1 is the sum of three terms:

$$Q_{in} = Q_{reservoir} + Q_{rear} + Q_{overflow} \quad (2)$$

where $Q_{reservoir}$ is the flow through Section S_2, Q_{rear} is the flow through Section S_3 and $Q_{overflow}$ is the reflected overflow outgoing from the reservoir (Figure 6). The water effectively collected in the reservoir, generating the $Q_{turbine}$.

In Figure 7, the non-dimensional time average wave overtopping per meter width:

$$q^*_{reservoir} = \frac{q_{reservoir}}{\sqrt{g \times H^3_{m0}}} \quad (3)$$

is plotted against the relative crest free-board:

$$R^*_r = \frac{R_r}{H_{m0}} \quad (4)$$

where $q_{reservoir}$ is the time average wave overtopping per meter width. The point data refer to tests with R_r = 0.125 m.

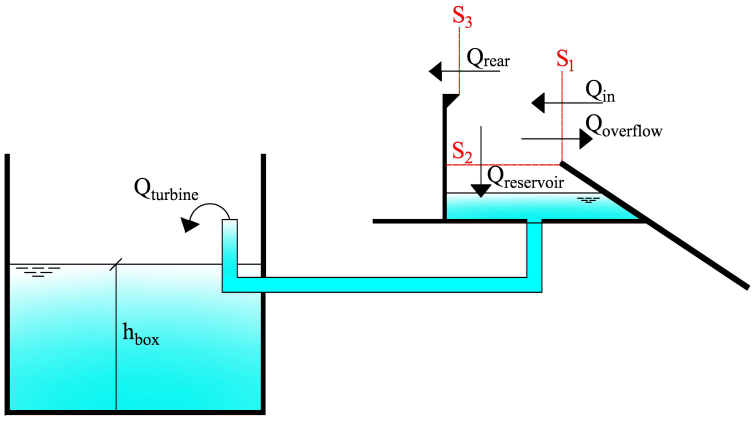

Figure 6. Definition of the overtopping input.

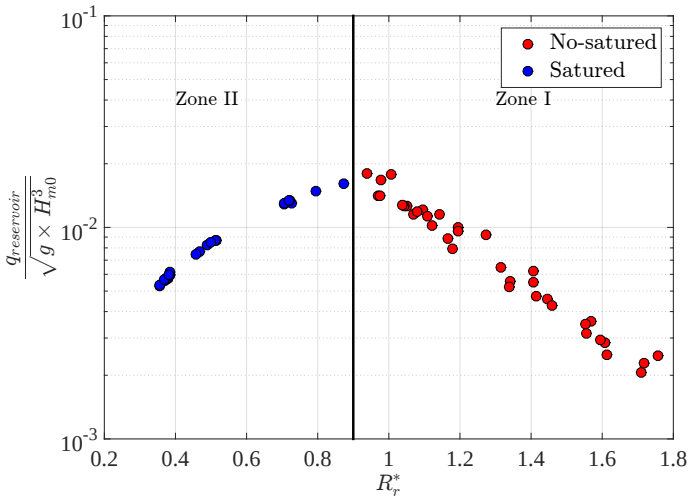

Figure 7. Non-dimensional average wave overtopping as function of R_r^*. The point data refer to tests with R_r = 0.125 m.

Two zones could be clearly identified: in Zone I, $q^*_{reservoir}$ increases with the decreasing of R_r^*; in Zone II, the $q^*_{reservoir}$ decreases with the decreasing of R_r^*. The trend observed in Zone I is typical of an overtopping process. In this zone, Q_{rear} and $Q_{overflow}$ are null, and $\bar{Q}_{in} = \bar{Q}_{reservoir} = \bar{Q}_{turbine}$ (the overbar represent the time average values).

Zone II identifies a range where the reservoir operates in a saturated condition. In such a condition, a large volume of water is lost (i.e., $Q_{overflow}$ increases). For this reason, $q^*_{reservoir}$ decreases with the decreasing of R_r^*. In this zone, $\bar{Q}_{in} > \bar{Q}_{reservoir}$ and $\bar{Q}_{reservoir} = \bar{Q}_{turbine}$.

The overtopping rate observed in Zone II is strongly affected by test-specific conditions (e.g., reservoir dimensions, localized and distributed load losses, hole geometry). For this reason, the overtopping rate observed in Zone II will not be taken into account in the analysis. Therefore, the following sections describe the results obtained in Zone I.

3.1. Overtopping Discharge in the Front Reservoir

The wave overtopping in the front reservoir can be analyzed as in the case of structures with a single slope. For these types of structure, in the case of no breaking wave, the wave overtopping q can be expressed as by the functional relationship f:

$$q = f\left(g, H_{m0}, R, \gamma\right) \tag{5}$$

where R indicates the crest free-board of the structure and γ indicates a coefficient that takes into account all of the factors that reduce the wave overtopping.

In EurOtop Manual [30], the average dimensionless overtopping discharge per meter structure width is estimated as:

$$\frac{q}{\sqrt{g \times H_{m0}^3}} = c_1 \times exp\left(-c_2 \frac{R}{H_{m0}} \times \frac{1}{\gamma_f \times \gamma_\beta \times \gamma_b}\right) \quad (6)$$

where: c_1 and c_2 are empirical coefficients; γ_f is the influence factor for the permeability and roughness of the slope; γ_β is the influence factor for the oblique wave attack; γ_b is the influence factor for a berm. The coefficient c_1 is equal to 0.2, while c_2 is equal to 2.6 for the probabilistic method and 2.3 for the deterministic method. Equation (6) was extended by Victor and Troch [31] in the case of an impermeable slope. In particular, Victor and Troch [31] have estimated the values c_1 and c_2 as a function of the slope angle of the structure, the crest free-board and the significant wave height. The authors observed that the effect of the wave period can be neglected due to non-breaking waves on the slope.

Based on the AAU12 tests, Vicinanza et al. [8] proposed a new formula to estimate the average dimensionless overtopping discharge. The formula was developed on the basis of the tests conducted for two configurations of OBREC. In particular, two different lengths of the ramp (d_w) were tested (Section 2.2 provides a description of the geometrical and wave characteristics of the AAU12 tests). The equation proposed by Vicinanza et al. [8] is the following:

$$\frac{q_{reservoir}}{\sqrt{g \times H_{m0}^3}} = 10^{-3}\left(35.1 + 2.38\frac{d_w}{\Delta R_c}\right) exp\left[\left(-58.99 + 17.7\frac{d_w}{\Delta R_c}\right) s_{Rr}\right] \quad (7)$$

where the parameter s_{Rr} is named the wave-structure steepness:

$$s_{Rr} = \frac{R_r}{H_{m0}} \times \frac{R_r}{L_{m0}} \quad (8)$$

The application range of Equation (7) is $0.64 < \frac{d_w}{\Delta R_c} < 1.35$ and $0.0123 < s_{Rr} < 0.202$ [8].

Figure 8 shows the comparison between the measured non-dimensional average front reservoir overtopping discharge and the prediction methods: (a) Vicinanza et al. [8]; (b) EurOtop Manual [30].

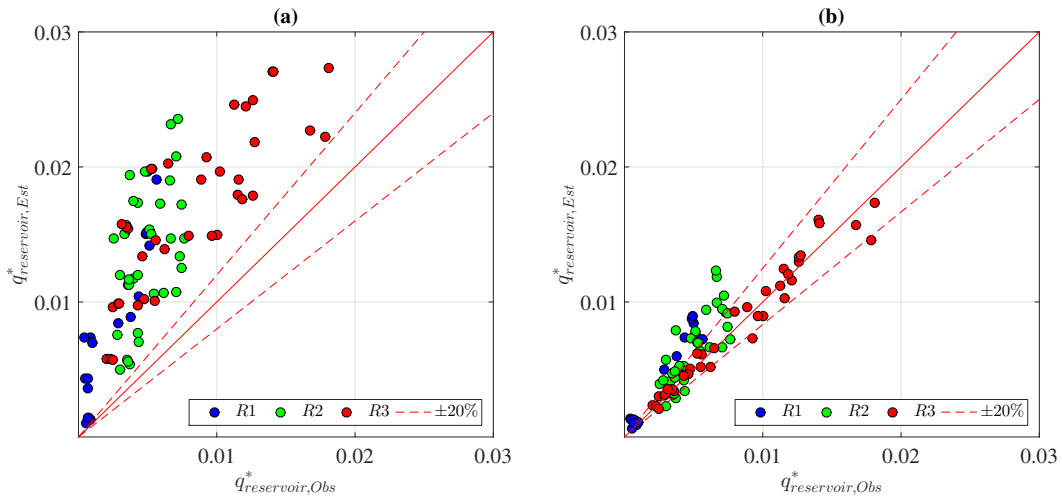

Figure 8. Comparison between the measured non-dimensional average front reservoir overtopping discharge and prediction methods: (**a**) Vicinanza et al. [8]; (**b**) EurOtop Manual [30].

The prediction methods' reliability is expressed using the root-mean square error (*rmse*), defined by the following relationship:

$$rmse = \sqrt{\frac{1}{N} \times \sum_{k=1}^{N} \left[\log q^*_{Obs} - \log q^*_{Est}\right]^2} \quad (9)$$

where N is the number of the test, q^*_{Obs} is the dimensionless overtopping discharge observed and q^*_{Est} is the dimensionless overtopping discharge estimated using the prediction method.

The Vicinanza et al. [8] formula overestimates the observed values. Indeed, the *rmse* values are: 8.23 for $R1$, 7.90 for $R2$ and 7.71 for $R3$. The reason is straightforward and addressable by the significant difference in the model setup of the AAU12 and AAU14 tests (Figures 3 and 4; Table 1). Indeed, the AAU12 model was equipped with a toe berm, and the submerged ramp was absent (i.e., new configurations are out of the range of application of Equation (7)).

The formula of EurOtop Manual [30] fits quite well the observed values using $\gamma_f = 1$. The *rmse* values are: 0.47 for $R1$, 0.22 for $R2$ and 0.01 for $R3$. However, a more detailed analysis shows that the decrease of d_d leads to a difference between the observed values and the values estimated using Equation (6). This behavior is due to the effect of the amour roughness. It was observed that the shorter the height of the submerged sloping plate (d_d) with respect to the wavelength, the larger the effect of the amour roughness. This aspect can be clarified observing Figure 9, which shows the ratio between the dimensionless measurement overtopping discharge and the one estimated by Equation (7) using $\gamma_f = 1$.

More in detail, the effect of the amour roughness is negligible for $d_d/L_{m-1,0} > 0.05$, and Equation (7) with $\gamma_f = 1$ predicts the observed overtopping discharge with enough accuracy (the spread is ±20%). For $d_d/L_{m-1,0} < 0.05$, the effect of the amour roughness is very relevant, and Equation (7) with $\gamma_f = 1$ overestimates the overtopping discharge.

Bruce et al. [32] estimated γ_f for various types of homogeneous armor units. For a composite structure, as OBREC, a constant value of γ_f cannot be defined, but such a parameter has been evaluated according to the incident wave characteristics and to the length of submerged ramp.

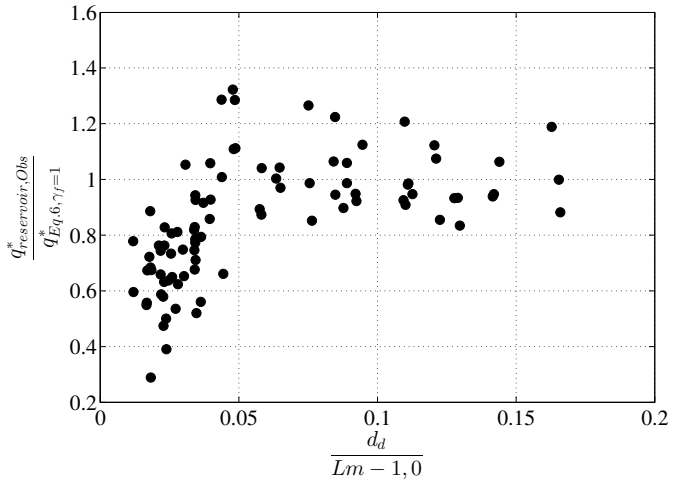

Figure 9. Comparison between the dimensionless measurement overtopping discharge and the one estimated by Equation (7) using $\gamma_f = 1$.

In order to evaluate the effect of the amour roughness for the analyzed configurations, γ_f, which minimize the differences between the values of $q_{reservoir}$ observed and those estimated with the EurOtop Manual [30] relationship (Equation (6)), was estimated (see Figure 10), and a relationship between γ_f and the relative ramp depth $\frac{d_d}{L_{m-1,0}}$ was determined:

$$\gamma_f = \begin{cases} tanh\left(s_1\left(\frac{d_d}{L_{m-1,0}}\right)^{s_2}\right) & if\ \frac{d_d}{L_{m-1,0}} > 0.006 \\ 0.7 & if\ \frac{d_d}{L_{m-1,0}} < 0.006 \end{cases} \quad (10)$$

where $s_1 = 7.47$ and $s_2 = 0.42$. The lower limit $\gamma_f = 0.7$ was detected by analyzing the AAU12 tests, which were performed with d_d close to 0 m. Indeed, for such tests, it was observed that Equation (6) can be applied adopting values of 0.7 for γ_f [8].

Figure 10a shows also the comparison between the value of γ_f estimated on the basis AAU14 tests and predicted values by Equation (10). Figure 10b shows the comparison between the $q_{reservoir}$ observed and $q_{reservoir}$ estimated with Equation (6) using the γ_f computed from Equation (10).

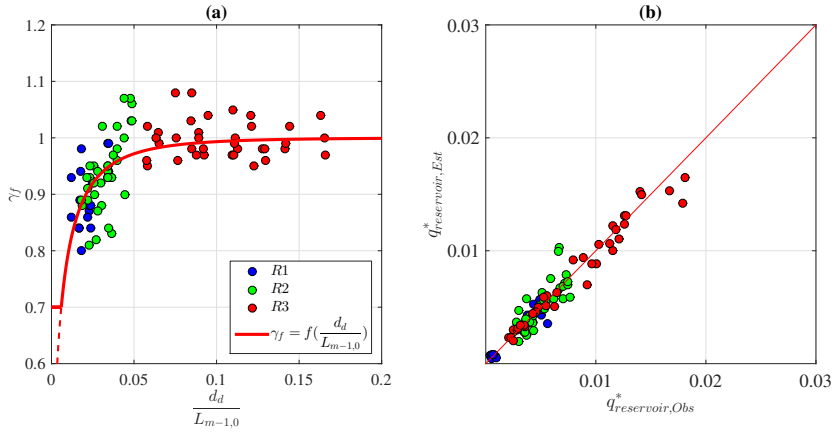

Figure 10. Overtopping discharge in the front reservoir: (**a**) comparison between γ_f estimated on the basis of the AAU14 tests and predicted values by Equation (10); (**b**) comparison between the $q_{reservoir}$ observed and $q_{reservoir}$ estimated with Equation (6) by using the γ_f computed from Equation 10. In (**b**) the red line indicates the perfect matching between the two quantities.

Comparisons of $q^*_{reservoir}$ between flat and curved configurations are presented in Figure 11. As can be seen from Table 1, the ramp crest free-board (R_r) of the flat configuration is 4 mm greater than the curved configuration. Hence, in order to make the comparisons more reliable, non-dimensional overtopping rates in Figure 11 are divided by the relative crest free-board. The comparison shows that the curved configuration gives approximately 22% less overtopping than the flat configuration.

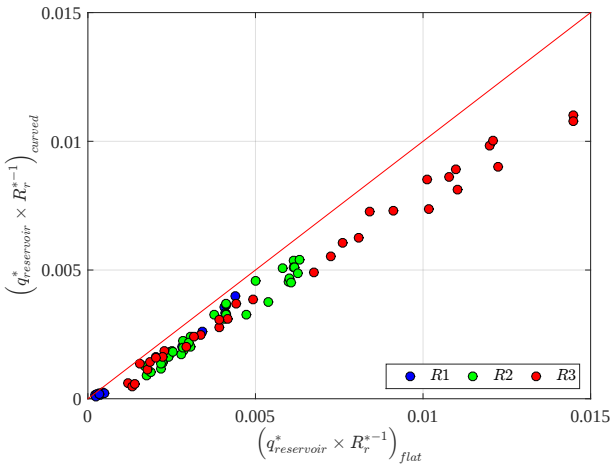

Figure 11. Overtopping into the front reservoir: $q^*_{reservoir}/R^*_r$ observed in the presence of the flat configuration versus $q^*_{reservoir}/R^*_r$ observed in the presence of the curved configuration.

3.2. Reflection

Several previous studies have been performed to analyze the reflection caused by coastal structures. Some of these studies have enabled the development of new prediction methods to estimate the reflection coefficient K_r, i.e., the ratio between reflected ($H_{m0,r}$) and incident wave heights ($H_{m0,i}$).

For rubble mound breakwater, the reflection coefficient can be expressed by the following functional relationship:

$$K_r = f\left(\alpha, H_{m0}, L_{m-1,0}, \gamma_f\right) \tag{11}$$

where α is the structure slope angle and $L_{m-1,0}$ is the deep water wavelength estimated with reference to $T_{m-1,0}$ at the structure toe.

Recently, Zanuttigh and van der Meer [33] have developed a new estimation formula for various types of structures. This formula allows one to estimate K_r once known: incident wave characteristics (H_{m0} and $T_{m-1,0}$) at the structure toe, the slope of the structure (α) and roughness coefficient γ_f:

$$K_r = tanh\left(a \times \xi_{m-1,0}^{b}\right) \tag{12}$$

where $\xi_{m-1,0}$ is the breaking parameter and the coefficients a and b are defined by the following relationship:

$$\begin{aligned} a &= 0.167 \times \left[1 - exp(3.2 \times \gamma_f)\right] \\ b &= 1.49 \times (\gamma_f - 0.38)^2 + 0.86 \end{aligned} \tag{13}$$

Vicinanza et al. [8] suggested the adoption of Equation (12) for the estimation of K_r. This method, in fact, appears opportunely conservative. In more detail, the analysis showed a good agreement between the predicted and the observed K_r adopting a γ_f value equal to 0.55. Moreover, for the configuration in the AAU12 tests with greater $q^*_{reservoir}$, a reduction of K_r was recognized. This behavior was explained by the fact that the device captures the incoming wave energy. Such an aspect was also observed for breakwaters by Zanuttigh and van der Meer [33], as the lower the crest, the greater the overtopping and the lower the reflection. In order to take into account such behavior, the authors introduce a reduction factor of the reflection coefficient:

$$\gamma_{K_r} = (0.67 + 0.37 \times R^*) \quad for -1 < R^* < 0.5 \tag{14}$$

where R^* is the relative crest free-board of the structure. Equation (14) was estimated for rock permeable slopes, and it can be applied to the following range: $R^* \geq -1$; $H_{m0}/D_{n50} \geq 1$; and $s_{m-1,0} \geq 0.01$.

Figure 12 shows the comparison between the reflection coefficients ($K_{r,obs}$) measured in the AAU14 tests and those estimated with Equations (12) and (13) ($K_{r,est}$). A good correspondence can be found. In particular, the value of $K_{r,est}$ is estimated using three different values of γ_f with the variation of the water level: 0.55 for $R1$; 0.8 for $R2$; and 0.9 for $R3$.

As can be seen from Figure 12, an increasing of the submerged ramp length (d_d) causes an increase of reflection. This aspect is consistent with the observation of the the higher overtopping discharges due to the decrease of the armor roughness observed in the previous section.

In order to take into account also the effect of the submerged ramp length, a new prediction method based on Equation (12) has been derived. Using the values of γ_f estimated from Equation (10), the method of Zanuttigh and van der Meer [33] overestimates the experimental data. Such behavior is caused by the structural difference between the models used by Zanuttigh and van der Meer [33] and the OBREC. Therefore, to evaluate K_r, a corrective coefficient was introduced:

$$\gamma_{f,K_r} = c_{\gamma_f} \times \gamma_f \tag{15}$$

with γ_f estimated by Equation (10) and c_{γ_f} evaluated through the following relationship:

$$c_{\gamma_f} = tanh\left(s_{1,r} \times X_{Kr}^{s_{2,r}}\right) \tag{16}$$

where $s_{1,r}$ = 2.64 and $s_{2,r}$ = 0.28, and X_{Kr} is defined as:

$$X_{K_r} = \frac{R_r}{H_{m0}} \times \frac{d_d}{L_{m-1,0}} \tag{17}$$

The parameters $s_{1,r}$ and $s_{2,r}$ were evaluated by the fitting process using the least squares method.

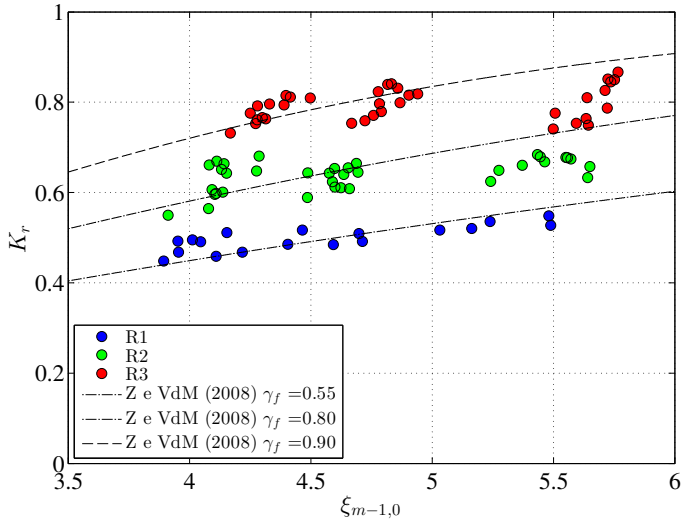

Figure 12. Comparison between the measured K_r in the AUU14 test and those estimated by Equation (12).

Figure 13a shows the comparison between c_{γ_f} detected by experiments and the calculated values with Equation 16. Figure 13b shows the comparison between K_r observed and K_r estimated with Equations (12), (13) and (15).

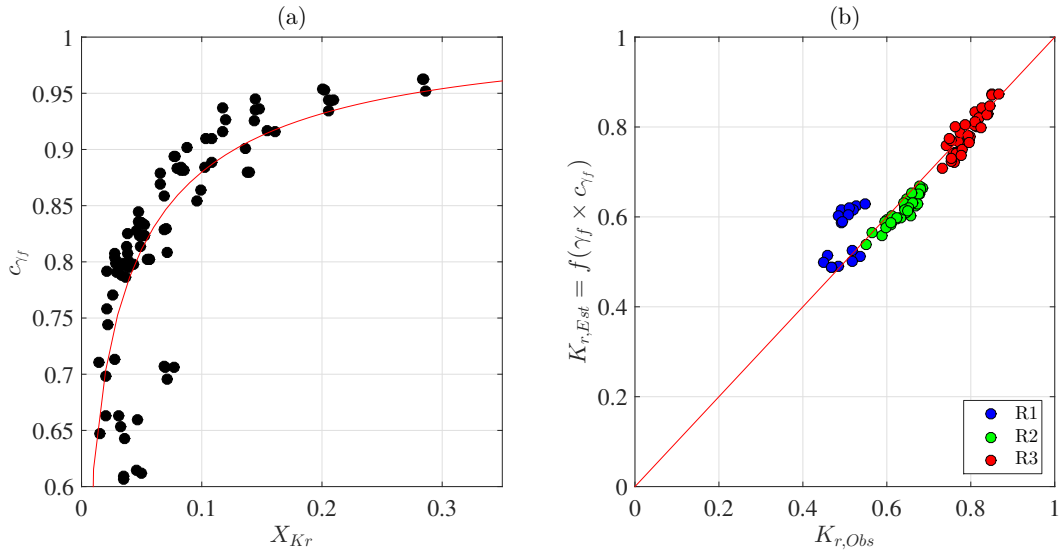

Figure 13. Prediction formula: (**a**) comparison between c_{γ_f} detected by experiments and the calculated values with Equation 16; (**b**) comparison between K_r observed and K_r estimated with Equations (12), (13) and (15).

Figure 14 shows the values of K_r as a function of the breaking parameter ($\xi_{m-1,0}$) classified depending on R_r and on the ramp shape (flat and curved). The comparison shows that for large values of R_r (cases $R1$ and $R2$), the difference between the flat configuration and curved configuration is negligible. Such a difference becomes relevant for the case with small values of R_r, that is $R3$. This behavior is because: the reflection coefficient tends to increase with the slope. In fact, near the ramp crest, the curved configuration has a slope smaller than the flat configuration, causing an attenuation in reflection.

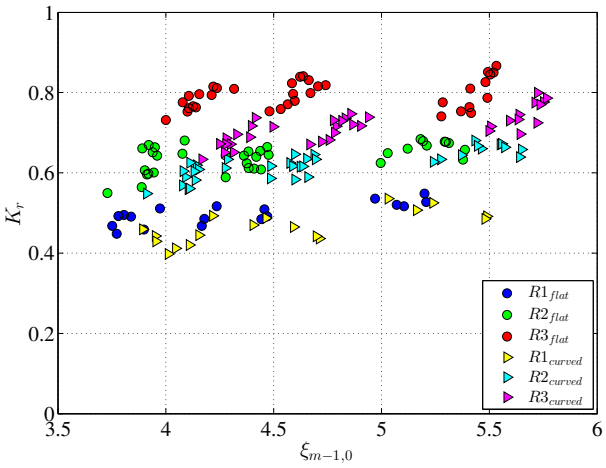

Figure 14. Reflection coefficient: comparison between the flat and the curved configurations.

3.3. Wave Overtopping at the Rear Side of the Structure

Coastal engineers design breakwaters generally with the main aim to limit the overtopping discharge at the rear side of the crown wall.

OBREC can be considered as a slope with a crown wall provided with a parapet. For this type of structure, there were no specific studies before the AAU12 tests. In order to address this shortcoming, Vicinanza et al. [8] developed a new prediction formula:

$$\frac{q_{rear}}{\sqrt{g \times H_{m0}^3}} = \frac{6.47}{1000} \times exp\left[-112 \times \left(\frac{R_c}{H_{m0}} \times \frac{\Delta R_c}{L_{m-1,0}}\right)\right] \quad (18)$$

where ΔR_c is the difference between R_c and R_r. The range of application of Equation (18) is: $0.014 < \frac{\Delta R_c}{L_{m-1,0}} < 0.038$; $0.035 < s_{m-1,0} < 0.058$; $1.24 < \frac{R_c}{H_{m0}} < 1.38$ [8].

Van Doorslaer et al. [34] analyzed several configurations to reduce the wave overtopping over the smooth dike slope. The authors extended the prediction method of EurOtop Manual [30] (Equation (6)) for structures very similar to OBREC. One of these structures is composed of a promenade and a storm wall, and another one is composed of a promenade, a storm wall and a parapet. The authors have modified the EurOtop Manual [30] formula as:

$$\frac{q}{\sqrt{g \times H_{m0}^3}} = 0.2 \times exp\left(-2.3 \frac{R_c}{H_{m0}} \times \frac{1}{\gamma_{VD}}\right) \quad (19)$$

where γ_{VD} is defined as:

$$\gamma_{VD} = 0.87 \times \gamma_v \times \gamma_{prom} \quad (20)$$

for a smooth breakwater with a promenade and a storm wall, and as:

$$\gamma_{VD} = 1.03 \times \gamma_v \times \gamma_{par} \times \gamma_{prom} \quad (21)$$

for a smooth breakwater with a promenade, a storm wall and a parapet, where the coefficients γ_v, γ_{par}, γ_{prom} take into account respectively the reduction effect of the storm wall, the reduction effect of the parapet and the reduction effect of the promenade. Methods for reduction factors' estimation are shown in Van Doorslaer et al. [34].

Figure 15 shows the comparison between the observed values and the Equation (18). The overtopping discharge for configuration $\Delta B_{rs} = 0.30$ m is estimated fairly well by Equation (18), while for configurations $\Delta B_{rs} = 0.10$ m and $\Delta B_{rs} = 0.20$ m, overtopping is underestimated. Such behavior is because of the fact that Equation (18) does not take into account the effects of the reservoir width.

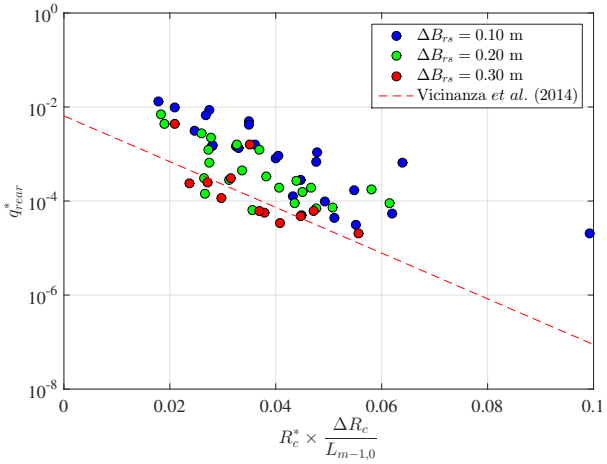

Figure 15. Comparison between the observed overtopping discharge and Equation (18).

AAU14 measured discharges versus computed values by Equation (19) for two different configurations tested by Van Doorslaer et al. [34] are reported in Figure 16a,b. For the structure without a parapet, Equation (19) interprets quite well the experimental data for $\Delta B_{rs} = 0.20$ m. However, for $\Delta B_{rs} = 0.10$ m and $\Delta B_{rs} = 0.30$ m, the average overtopping discharges are respectively underestimated and overestimated. For the structure with a parapet (Figure 16a,b), the approach of Van Doorslaer et al. [34] tends to underestimate the measured values. The main reason for these discrepancies can be explained by the absence of the reservoir.

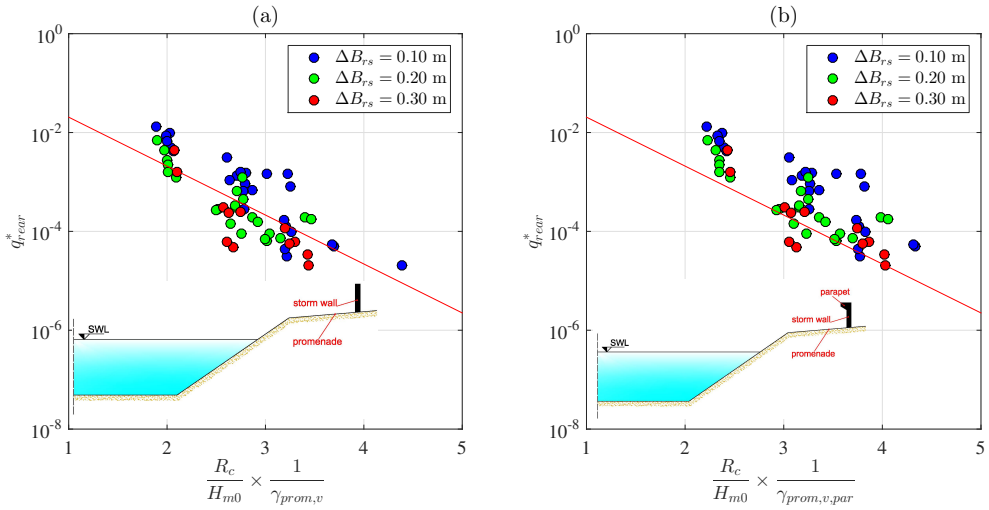

Figure 16. Comparison between the observed values and Equation (19) ($\gamma_v = 0.78$; $\gamma_{par} = 0.72$): (**a**) the case of the structure without a parapet; (**b**) the case of the structure with a parapet.

Table 4 shows the performances of the two prediction methods.

Table 4. Prediction method performances. The *rmse* was estimated using Equation (9).

Type Structures	Vicinanza et al. [8] OBREC	Van Doorslaer et al. [34] Promenade-Storm Wall	Van Doorslaer et al. [34] Promenade-Storm Wall-Parapet
$\Delta B_{rs} = 0.10$ m	2.77	1.28	2.21
$\Delta B_{rs} = 0.20$ m	1.65	0.79	1.20
$\Delta B_{rs} = 0.30$ m	1.08	1.13	0.93

Based on the AAU14 tests, a new prediction method was developed. The average wave overtopping can be expressed by the following functional relationship:

$$q_{rear} = f\left(H_{m0}, L_{m-1,0}, R_c, \Delta B_{rs}, d_w, R_r\right) \tag{22}$$

This expression can be arranged in terms of dimensionless parameters:

$$\frac{q_{rear} \times T_{m-1,0}}{L^2_{m-1,0}} = f\left(\frac{R_c}{H_{m0}}, \frac{\Delta B_{rs}}{Br}, \frac{\Delta R_c}{d_w}\right) \tag{23}$$

On the basis of the AAU14 tests with the flat ramp, the overtopping discharge at the rear side of the breakwater could be evaluated by the following relation:

$$\frac{q_{rear} \times T_{m-1,0}}{L^2_{m-1,0}} = a_{rear} \times exp\left(b_{rear} \times X_{rear}\right) \tag{24}$$

where a_{rear} = 0.0139 and b_{rear} = −7.17, and the parameter X_{rear} is defined by the following equation:

$$X_{rear} = \frac{R_c}{H_{m0}} \times \left(\frac{\Delta B_r}{B_r}\right)^{0.5} \times \left(\frac{\Delta Rc}{d_w}\right)^{0.25} \tag{25}$$

The parameters a_{rear} and b_{rear} were evaluated by the fitting process using the least squares method.

Figure 17 shows the comparison between the measured overtopping discharges and calculated from Equation (24). Experimental data are excellently interpreted by Equation (24) with a good correlation coefficient ($R^2 > 0.96$) and an *rmse* = 0.69.

In order to make a comparison and to establish the reliability of Equation (24), AAU12 data are also reported in Figure 17.

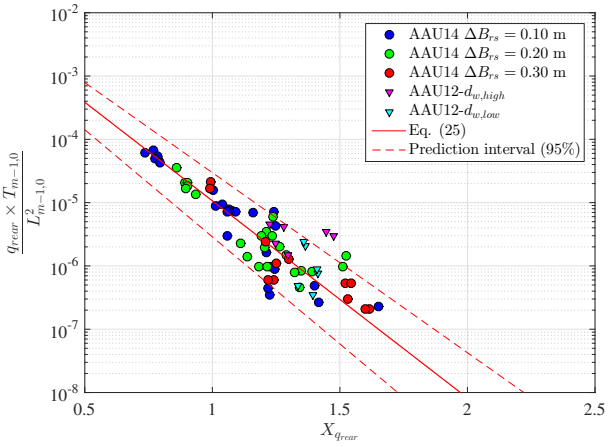

Figure 17. Comparison between Equation (24) and the data observed in the AAU14 tests with a flat ramp and the AAU12 tests.

The new formula can also be applied to the curved configuration by adopting an appropriate correction factor. Indeed, the curved shape of the ramp causes less wave overtopping discharge than the flat configuration. A mean difference of approximately 20% was estimated. Therefore, a new correction factor $\gamma_{q_{rear}}$ was introduced. Such a factor equals one for the flat configuration and 0.83 for the curved configuration. Equation (24) can be rewritten as:

$$\frac{q_{rear} \times T_{m-1,0}}{L_{m-1,0}^2} = a_{rear} \times exp\left(b_{rear} \times \frac{X_{rear}}{\gamma_{q_{rear}}}\right) \quad (26)$$

The comparison between the observed values (flat and curved configurations) and those estimated using Equation (26) is shown in Figure 18.

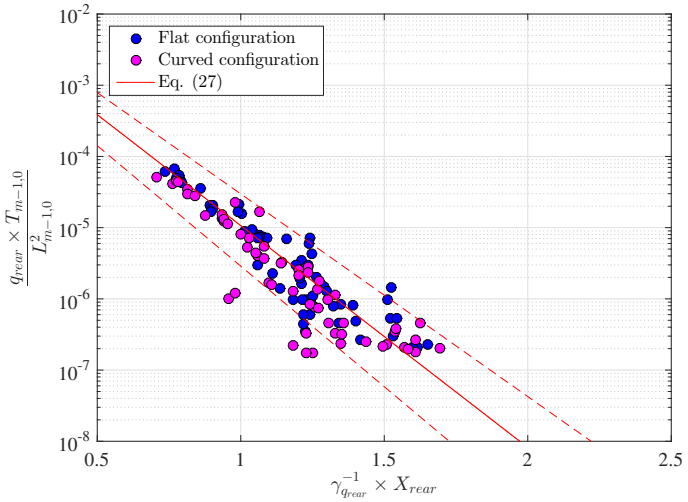

Figure 18. Overtopping at the rear of the structure: comparison between Equation (26) and the observed values during the AAU14 tests (flat and curved configurations).

4. Conclusions

This paper presents a study of the innovative Overtopping BReakwater for wave Energy Conversion (OBREC). Moving on from the complementary tests by Vicinanza et al. [8], 2D model tests were carried out at Aalborg University. The main purpose of this new experimental campaign was to extend the knowledge on the device behavior, with particular interest in the influence of the shape and draft of the front ramp, as well as the reservoir width. This parametric study aims to bring completion to the previous one in which different ramp crest elevations were tested.

Two different device configurations are analyzed: the first is characterized by a constant slope ramp; the second presents a curved ramp profile. For both configurations, tests with three different reservoir widths and three water levels were considered.

Wave overtopping in the front reservoir could be predicted by the method of EurOtop Manual [30] with a relatively accurate estimation. However, due to the dual nature of OBREC, a high level of accuracy in overtopping discharge effectively usable for energy production is required. Thus, a new method to estimate the roughness factor as a function of the submerged ramp length and the wavelength was developed.

As regards the reflection coefficient, the two tested configurations show the same behavior. However, the reflection coefficients measured in the previous test campaign were lower than the present ones. Such a behavior is mainly caused by the different extension of the submerged ramp. The prediction method of Zanuttigh and van der Meer [33] can be used to estimate wave reflection, although it is necessary to apply a correction factor as a function of the wave characteristics and some geometrical characteristics of the ramp.

A reduction of approximately 20% in overtopping rates in the front reservoir and at the rear side of the structure was observed for the curved configuration. This could significantly affect the potential energy production of the system, but at the same time, a higher safety level at the rear side of the crown wall can be ensured in comparison to the flat configuration.

A new prediction method to estimate overtopping discharge at the rear side of the structure was proposed, which was proven to perform remarkably well with respect to the present dataset. Based on the approach proposed by Vicinanza et al. [8], the new formula allows one to take into account the effects of the reservoir width.

The analysis described in this paper represents a further step forward in the knowledge of the OBREC device. Future studies will mainly focus on the evaluation of the energy production performance and how it can be affected by the geometrical characteristics of the device (width and depth of the reservoir, height of sloping plate, etc.) and by the turbine characteristics.

Acknowledgments: The work discussed here is a part of the National Operational Programme for the "Research and Competitiveness" 2007–2013 (NOP for R&C) founded Project PON04a3_00303 titled "DIMEMO-DIgaMarittima per l'Energia del Moto Ondoso" (Maritime Breakwater for Wave Energy Conversion), Project PON04a3_00303. The work also was partially supported by RITMARE (acronym of la Ricerca ITaliana per il MARE) Flagship Project and by the project PON02_000153_2939551 "Development of innovative technologies for energy saving and environmental sustainability of shipyards and harbor areas" (SEAPORT, acronym of Sviluppo di tecnologie innovative per la Sostenibilità Energetica ed Ambientale di cantieri navali ed aree PORTuali) and by HYDRALAB PLUS project (Proposal Number 64110). The authors gratefully acknowledge the Italian Ministry of Education, University and Research for supporting this innovative research and the Second University of Naples and the University of Catania for encouraging the mobility of researchers. Important input from Thomas Lykke Andersen in the study design and data analyses is gratefully acknowledged. The authors would also like to thank the Aalborg University technicians, in particular Niels Drustrup, for their cheerfulness, tolerance and considerable assistance in the design evolution, model construction and testing. Assistance in the testing and supporting physical modeling from Vincenzo Ferrante (Second University of Naples) is also gratefully acknowledged.

Author Contributions: Claudio Iuppa contributed to the work described in this paper by collaborating in carrying out the laboratory campaign and analyzing the acquired data. Pasquale Contestabile contributed to the work by designing and collaborating in carrying out the laboratory campaign and analyzing the acquired data. Luca Cavallaro contributed to the work by analyzing the acquired data. Enrico Foti contributed with knowledgeable discussion and suggestion. Diego Vicinanza gave the idea, supervised the data analyses and gave the final approval. All of the co-authors participated in writing the paper.

Conflicts of Interest: The authors declare no conflict of interest.

Nomenclature

B_r (m)	reservoir width
B_s (m)	emerged sloping plate width
d_d (m)	height of the submerged sloping plate
D_{n50} (m)	equivalent cube side length exceed by 50% of the stones
d_w (m)	height of sloping plate
g $(m \cdot s^{-2})$	gravity acceleration
h (m)	depth at the toe of the structure
h_{box} (m)	depth in the accumulation box
$H_{m0,r}$ (m)	reflected significant wave height at the toe of the structure
H_{m0} (m)	incident significant wave height at the toe of the structure
h_r (m)	depth in the front reservoir
K_r (-)	$\frac{H_{m0,r}}{H_{m0}}$ reflection coefficient
$L_{m-1,0}$ (m)	deep water wavelength referenced to $T_{m-1,0}$
m_0 (m^2)	spectral moment of order 0
m_{-1} $(m^2 \cdot s)$	spectral moment of order -1
q^*_{rear} (-)	non-dimensional overtopping discharge towards the rear of the traditional rubble mound breakwater crown wall or towards the rear OBREC crown wall
$q^*_{reservoir}$ (-)	non-dimensional overtopping discharge into the reservoir
q_{rear} $(m^3 \cdot m^{-1} \cdot s^{-1})$	average overtopping discharge towards the rear of the traditional rubble mound breakwater crown wall or towards the rear of the OBREC crown wall

$q_{reservoir}$ $[m^3 \cdot m^{-1} \cdot s^{-1}]$	average overtopping discharge into the reservoir
R [m]	crest free-board of the structure
$R_c^* = \frac{R_c}{H_{m0}}$ [-]	relative crest free-board of crown wall
$R_r^* = \frac{R_r}{H_{m0}}$ [-]	relative crest free-board of front reservoir
R_c [m]	crest free-board of crown wall, i.e., the vertical distance between the crest of the vertical walland the still water level
R_r [m]	crest free-board of front reservoir, i.e., the vertical distance between the crest of the sloping plate and the still water level
$rmse$ [-]	root mean square error
$s_{m-1,0} = \frac{2\pi H_{m0}}{gT_{m-1,0}^2}$ [-]	wave steepness at the toe of the structure
s_{Rr} [-]	non-dimensional wave-structure steepness
$T_{m-1,0} = \frac{m_{-1}}{m_0}$ [s]	spectral incident energy wave period at the toe of the structure
T_p [s]	incident peak wave period
α [°]	slope angle of the structure
γ [-]	peak-enhancement factor
γ_β [-]	reduction factor for oblique wave attack
γ_b [-]	reduction factor for berm
γ_f [-]	reduction factor for slope roughness
γ_v [-]	reduction factor for the storm wall
γ_{par} [-]	reduction factor for the parapet
γ_{prom} [-]	reduction factor for the promenade
ρ $[kg \cdot m^{-3}]$	water density
$\xi_{m-1,0} = \frac{tan\alpha}{s_{m-1,0}^{0.5}}$ [-]	breaker parameter referenced to $T_{m-1,0}$
$\Delta B_{rs} = B_r - B_s$ [m]	horizontal distance between the crown wall and the crest of the ramp
$\Delta R_c = R_c - R_r$ [m]	vertical distance between the crown wall and the crest of the ramp

References

1. Mofor, L.; Goldsmith, J.; Jones, F. *OCEAN ENERGY: Technology Readiness, Patents, Deployment Status and Outlook*; International Renewable Energy Agency (IRENA): Masdar City, United Arab Emirates, 2014.
2. Pastor, J.; Liu, Y. Power absorption modeling and optimization of a point absorbing wave energy converter using numerical method. *J. Energy Resour. Technol.* **2014**, *136*, 021207.
3. Drew, B.; Plummer, A.; Sahinkaya, M.N. A review of wave energy converter technology. *Proc. Inst. Mech. Eng. A. J. Power Energy* **2009**, *223*, 887–902.
4. Azzellino, A.; Conley, D.; Vicinanza, D.; Kofoed, J.P. Marine renewable energies: Perspectives and implications for marine ecosystems. *Sci. World J.* **2013**, *2013*, doi:10.1155/2013/547563.
5. Peres, D.; Iuppa, C.; Cavallaro, L.; Cancelliere, A.; Foti, E. Significant wave height record extension by neural networks and reanalysis wind data. *Ocean Model.* **2015**, *94*, 128–140.
6. Falcão, A. Wave energy utilization: A review of the technologies. *Renew. Sustain. Energy Rev.* **2010**, *14*, 899–918.
7. Clément, A.; McCullen, P.; Falcão, A.; Fiorentino, A.; Gardner, F.; Hammarlund, K.; Lemonis, G.; Lewis, T.; Nielsen, K.; Petroncini, S.; et al. Wave energy in Europe: Current status and perspectives. *Renew. Sustain. Energy Rev.* **2002**, *6*, 405–431.
8. Vicinanza, D.; Contestabile, P.; Nørgaard, J.Q.H.; Andersen, T.L. Innovative rubble mound breakwaters for overtopping wave energy conversion. *Coast. Eng.* **2014**, *88*, 154–170.
9. Viviano, A.; Naty, S.; Foti, E.; Bruce, T.; Allsop, W.; Vicinanza, D. Large-scale experiments on the behavior of a generalised Oscillating Water Column under random waves. *Renew. Energy* **2016**, *99*, 875 – 887.
10. Pastor, J.; Liu, Y. Frequency and time domain modeling and power output for a heaving point absorber wave energy converter. *Int. J. Energy Environ. Eng.* **2014**, *5*, 1–13.
11. Vicinanza, D.; Nørgaard, J.H.; Contestabile, P.; Andersen, T.L. Wave loadings acting on overtopping breakwater for energy conversion. *J. Coast. Res.* **2013**, *65*, 1669–1674.
12. Iuppa, C.; Cavallaro, L.; Foti, E.; Vicinanza, D. Potential wave energy production by different wave energy converters around Sicily. *J. Renew. Sustain. Energy* **2015**, *7*, 061701.

13. Iuppa, C.; Cavallaro, L.; Vicinanza, D.; Foti, E. Investigation of suitable sites for wave energy converters around Sicily (Italy). *Ocean Sci.* **2015**, *11*, 543–557.
14. Kofoed, J.P.; Frigaard, P.; Friis-Madsen, E.; Sørensen, H.C. Prototype testing of the wave energy converter wave dragon. *Renew. Energy* **2006**, *31*, 181–189.
15. Vicinanza, D.; Frigaard, P. Wave pressure acting on a seawave slot-cone generator. *Coast. Eng.* **2008**, *55*, 553–568.
16. Margheritini, L.; Vicinanza, D.; Frigaard, P. SSG wave energy converter: Design, reliability and hydraulic performance of an innovative overtopping device. *Renew. Energy* **2009**, *34*, 1371–1380.
17. Vicinanza, D.; Ciardulli, F.; Buccino, M.; Calabrese, M.; Koefed, J. Wave loadings acting on an innovative breakwater for energy production. *J. Coast. Res.* **2011**, *64*, 608–612.
18. Vicinanza, D.; Margheritini, L.; Kofoed, J.P.; Buccino, M. The SSG wave energy converter: Performance, status and recent developments. *Energies* **2012**, *5*, 193–226.
19. Buccino, M.; Banfi, D.; Vicinanza, D.; Calabrese, M.; Giudice, G.D.; Carravetta, A. Non breaking wave forces at the front face of seawave slotcone generators. *Energies* **2012**, *5*, 4779–4803.
20. Veigas, M.; López, M.; Iglesias, G. Assessing the optimal location for a shoreline wave energy converter. *Appl. Energy* **2014**, *132*, 404–411.
21. Buccino, M.; Vicinanza, D.; Salerno, D.; Banfi, D.; Calabrese, M. Nature and magnitude of wave loadings at seawave slot-cone generators. *Ocean Eng.* **2015**, *95*, 34–58.
22. Contestabile, P.; Ferrante, V.; Di Lauro, E.; Vicinanza, D. Prototype Overtopping Breakwater for Wave Energy Conversion at Port of Naples. In Proceedings of the 26th International Conference ISOPE, Rhodes, Greece, 26 June–2 July 2016; pp. 616–621.
23. Vicinanza, D.; Stagonas, D.; Müller, G.; Nørgaard, J.H.; Andersen, T.L. Innovative breakwaters design for wave energy conversion. *Coast. Eng. Proc.* **2012**, *1*, doi:10.9753/icce.v33.structures.1.
24. Iuppa, C.; Contestabile, P.; Cavallaro, L.; Foti, E.; Lykke Andersen, T.; Vicinanza, D. Experimental investigation of rubble mound breakwaters for wave energy conversion. In Proceedings of the 11th European Wave and Tidal Energy Conference, Nantes, France, 6–11 September 2015; pp. 1–7.
25. Kofoed, J.P. *Experimental Hydraulic Optimization of the Wave Energy Converter Seawave Slot-Cone Generator*; Department of Civil Engineering, Aalborg University: Copenhagen, Denmark, 2005.
26. Kofoed, J.P. Wave Overtopping of Marine Structures: Utilization of Wave Energy. Available online: http://vbn.aau.dk/files/55289605/Wave_Overtopping-ofMarine_Structures_utilization_of_wave_energy.pdf (assesses on 19 November 2016).
27. Andersen, T.L.; Clavero, M.; Frigaard, P.; Losada, M.; Puyol, J. A new active absorption system and its performance to linear and non-linear waves. *Coast. Eng.* **2016**, *114*, 47–60.
28. Zelt, J.; Skjelbreia, J.E. Estimating incident and reflected wave fields using an arbitrary number of wave gauges. In *Coastal Engineering Conference;* American Society of Civil Engineers (ASCE): Reston, Virginia, 1992; Volume 1, p. 777.
29. Klopman, G.; van der Meer, J.W. Random wave measurements in front of reflective structures. *J. Waterw. Port Coast. Ocean Eng.* **1999**, *125*, 39–45.
30. EurOtop Manual. EurOtop—Wave Overtopping of Sea Defences and Related Structures–Assessment Manual. Available online: https://www.gov.uk/government/uploads/system/uploads/attachment_data/file/290261/scho0308bnvi-e-e.pdf (assessed online 19 November 2016).
31. Victor, L.; Troch, P. Wave overtopping at smooth impermeable steep slopes with low crest free-boards. *J. Waterw. Port Coast. Ocean Eng.* **2012**, *138*, 372–385.
32. Bruce, T.; Van der Meer, J.; Franco, L.; Pearson, J.M. Overtopping performance of different armor units for rubble mound breakwaters. *Coast. Eng.* **2009**, *56*, 166–179.
33. Zanuttigh, B.; van der Meer, J.W. Wave reflection from coastal structures in design conditions. *Coastal Eng.* **2008**, *55*, 771–779.
34. Van Doorslaer, K.; De Rouck, J.; Audenaert, S.; Duquet, V. Crest modifications to reduce wave overtopping of non-breaking waves over a smooth dike slope. *Coast. Eng.* **2015**, *101*, 69–88.